HUBBLE SPACE TELESCOPE METALLIZED TEFLON® FEP THERMAL CONTROL MATERIALS: ON-ORBIT DEGRADATION AND POST-RETRIEVAL ANALYSIS

J.A. Townsend[1], P.A. Hansen[1], J.A. Dever[2], K.K. de Groh[2],
B. Banks[2], L. Wang[3] and C. He[3]

1. NASA Goddard Space Flight Center, Greenbelt, Maryland, 20771 USA
2. NASA Lewis Research Center, Cleveland, Ohio 44135 USA
3. Unysis Corporation, Lanham, Maryland 20705 USA

ABSTRACT

During the Hubble Space Telescope (HST) Second Servicing Mission (SM2), degradation of unsupported Teflon® FEP (fluorinated ethylene propylene), used as the outer layer of the multi-layer insulation (MLI) blankets, was evident as large cracks on the telescope light shield. A sample of the degraded outer layer was retrieved during the mission and returned to Earth for ground testing and evaluation. The results of the Teflon® FEP sample evaluation and additional testing of pristine Teflon® FEP led the investigative team to theorize that the HST damage was caused by thermal cycling with deep-layer damage from electron and proton radiation which allowed the propagation of cracks along stress concentrations, and that the damage increased with the combined total dose of electrons, protons, UV and x-rays along with thermal cycling. This paper discusses the testing and evaluation of the retrieved Teflon® FEP.

1. INTRODUCTION

The Hubble Space Telescope was launched into Low Earth Orbit (LEO) in April 1990 with a mission to spend 15 years probing the farthest and faintest reaches of the cosmos. Crucial to fulfilling this promise is a series of servicing missions to upgrade scientific capabilities. During the First Servicing Mission (SM1) in December 1993, MLI blankets were retrieved and analyzed in ground-based facilities. These studies revealed that the outer layer of the MLI, aluminized Teflon® FEP, was beginning to degrade. Close inspection of the Teflon® FEP revealed through-thickness cracks in areas with the highest solar exposure and stress concentration. Mechanical tests showed significantly decreased ultimate strength and elongation [1].

During the Second Servicing Mission (SM2) in February 1997, astronauts observed and documented severe cracking in the outer layer of the MLI blankets on both solar facing and anti-solar facing surfaces [2]. During the repair process, a small specimen of the outer layer was retrieved from the Light Shield (LS) region and was returned for ground-based analysis. In addition, as part of an instrument installation, a sample of the bonded Teflon® FEP radiator surface was returned on the Cryogen Vent Cover (CVC).

Since the damage to the outer layer was so severe at SM2, a Failure Review Board was convened to, among other tasks, determine the mechanism of the damage. There were three phases to that investigation: document the condition of the MLI on the telescope; analyze the retrieved specimens; perform simulated

environmental exposures. This paper summarizes the results of the first two phases and draws overall conclusions about the failure mechanism.

2. HUBBLE SPACE TELESCOPE

2.1 Thermal Control Materials

2.1.1 Description

The Hubble Space Telescope uses several thermal control materials to passively control temperatures on-orbit. The two primary types are MLI blankets and radiator surfaces (Figure 1).

MLI blankets were used on over 80 percent of the external surface area of HST. The top (space-exposed) layer of these blankets was 127 μm (0.005 in) FEP with roughly 100 nm of vapor deposited aluminum (VDA) on the back (FEP/VDA). Next there were 15 layers of embossed 8.17 μm (0.00033 in) double-aluminized Kapton®. The inner-most layer was 24.5 μm (0.001 in) single aluminized Kapton. The embossing pattern reduced layer-to-layer conduction, making spacers unnecessary. The blankets were closed out on all four sides with a taped cap section, and the layers were tied together intermittently throughout the blanket using spots of acrylic transfer adhesive film. Where the blankets were cut to fit around features (handrails, standoffs, etc.) the blanket was closed out again by taping the cap section. In addition, the blankets were vented with "X" cuts and the outer layer was reinforced using aluminized Kapton® scrim tape. The entire blanket was attached to the spacecraft with Velcro® stitched to the inner layer.

The radiator surfaces were simply perforated silver Teflon® tape bonded directly to the aluminum vehicle substrate. The space-exposed surface was 127 μm (0.005 in) FEP with roughly 100 nm of vapor deposited silver (VDS) on the back (FEP/VDS). The silver side was coated with Inconel and finally with an acrylic adhesive. This material was purchased in rolls (4 in. width) with the adhesive already applied. The tape was applied in sections, and a Teflon® wand was used to minimize air entrapment and ensure a good bond. Damaged tape was replaced as necessary as the telescope was built.

2.1.2 Retrieved Specimens

Specimens of these thermal control materials were retrieved during the servicing missions. Table 1 provides the labels and descriptions of the specimens that will be discussed in this paper. No material was saved when the telescope was built, therefore no control material existed from the same production lot. The blanket shop at Lockheed Martin Missiles and Space (LMMS) provided a full-build MLI blanket in April 1997 to be used as the control sample for these analyses.

TABLE 1: SPECIMEN NAMES AND DESCRIPTIONS

Specimen Name	Description
Pristine	Outer layer MLI (FEP/VDA) from LMMS, received 4/15/97
SM1 MSS	Outer layer MLI (FEP/VDA) from magnetometer cover, retrieved at SM1, 12/93
SM2 LS	Outer layer MLI (FEP/VDA) from light shield region; retrieved at SM2, 2/97
SM2 CVC	Radiator surface (FEP/VDS) from cryogen vent cover; retrieved at SM2, 2/97

Complete MLI blankets were removed from the two magnetometers from the HST magnetic sensing system (MSS) during SM1 (Figure 2). The two

magnetometers were roughly cubic, and the covers had surfaces that received various solar exposures. A complete analysis of the damage at SM1 was performed by Zuby, de Groh, and Smith following the mission [1]. For the purpose of comparison with SM2 damage, a specimen of the top layer was cut from the section that received the middle range of solar exposure. When possible, SM1 results reported in this paper were taken from the earlier analysis of this section of the MSS covers. When an analysis had not been completed following SM1, the analysis was performed on this section along with the analysis of the SM2 specimen.

During SM2, a specimen from the outer layer of the MLI, shown in Figure 3, was taken from the upper light shield (LS) region of the telescope. The roughly triangular specimen was tightly curled, forming several rolled layers (Figure 3). The astronaut cut the specimen from right to left, with a change in the initial direction as the astronaut realized he was cutting through the roll of the specimen. In Figure 4 the specimen is shown flat with the cracks identified. The specimen was stored in a reclosable polyethylene bag and stowed in a mid-deck locker for the duration of the mission.

In addition to the outer layer MLI specimen, a radiator specimen was retrieved during SM2. As part of an instrument installation, a cryogen vent cover (CVC) was removed from the aft bulkhead and returned to Earth at project request. The outside of the CVC (radiator surface) had been exposed to the orbital environment and provided good data for the thermal degradation of the radiator surfaces.

2.2 Environment

The Hubble Space Telescope was deployed at an altitude of 598 km and an orbit inclination of 28.5 degrees. The telescope is oriented such that one side (+V3) faces the sun throughout its orbit, although the telescope does pitch and roll in order to maintain focus on a target object. This means that one side of HST (+V3) receives direct sunlight at all times when HST is not in the Earth's shadow, and the other side (-V3) only receives sunlight reflected from the Earth's surface (albedo). The other surfaces of the telescope receive varying amounts of sunlight depending on how much time is spent pointing in a given direction [2].

The exterior surfaces of HST are exposed to the orbital environment which includes solar radiation, charged particles (trapped particles and plasma), atomic oxygen, and temperature extremes. Solar exposure, including near ultraviolet radiation (UV), vacuum ultraviolet radiation, and soft x-rays from solar flares, may cause surface damage in polymeric materials such as Teflon® FEP. Higher energy soft x-rays from solar flares have the potential to penetrate and cause damage deep in the bulk of a material with sufficient fluence. Trapped electrons and protons (particle radiation) may cause molecular changes in the bulk of the material, changing the mechanical properties. Atomic oxygen can erode the surface through chemical reactions with gaseous oxide products. Temperature extremes and thermal cycling can enhance the rate of damage from other environmental factors, and in Teflon® FEP they can affect the molecular structure [1-4].

Table 2 contains a summary of the environmental exposure of each the retrieved specimens received in terms of fluence and, when appropriate, absorbed dose. The dose-versus-depth profile for each type of radiation was calculated, and the absorbed doses at 25.4 μm (0.001 in) and 127 μm (0.005 in) are included in Table 2. The total absorbed dose of ionizing radiation, included in the table, is the dose due to x-rays and trapped charged particles.

TABLE 2: ENVIRONMENTAL EXPOSURES FOR RETRIEVED HST MATERIALS

Environmental Factor	Deposited Depth	SM1 MSS	SM2 LS	SM2 CVC
Duration		3.6 years	6.8 years	
Atomic Oxygen (sweeping ram)		1.56E20 atoms/c m^2	1.64E20 atoms/c m^2	
Thermal Cycles				
Number of Cycles		19,800	37,300	37,300
Temperature Limits		-100 to +50 °C	-100 to 50 °C nominal -100 to 200 °C curled	-80 to -15 °C
Equivalent Sun Hours (ESH)		11,339 (7% albedo)	33,638 (0% albedo)	19,308 (33% albedo)
VUV Dose (<180 nm, absorbed)	1 mil	2.185E6 krads	6.480E6 krads	2.490E6 krads
	5 mil	4.37E5 krads	1.296E6 krads	4.98E5 krads
X-ray Fluence				
0.5 to 4 Å		8.7 J/m^2	16 J/m^2	6.1 J/m^2
1 to 8 Å		132 J/m^2	252 J/m^2	96.9 J/m^2
X-ray Dose				
0.5 to 4 Å	1 mil	0.98 krads	1.8 krads	0.69 krads
(24 to 3.1 keV)	5 mil	0.59 krads	1.1 krads	0.41 krads
1 to 8 Å	1 mil	59.1 krads	113.2 krads	43.4 krads
(12 to 1.55 keV)	5 mil	23.2 krads	44.4 krads	17.0 krads
Trapped Particle Fluence (> 40 keV)				
Electrons		1.39E13 #/cm^2	2.13E13 #/cm^2	
Protons		7.96E9 #/cm^2	1.83E10 #/cm^2	
Trapped Particle Dose (> 40 keV)				
Electrons	1 mil	277 krads	389 krads	
	5 mil	71.6 krads	95.9 krads	
Protons	1 mil	0.93 krads	2.32 krads	
	5 mil	0.75 krads	1.87 krads	
Plasma Fluence (.1 to a few keV; absorbed dose in 1 mil < 1 krad)				
Electrons		3.18E19 #/cm^2	4.66E19 #/cm^2	
Protons		1.11E19 #/cm^2	1.63E19 #/cm^2	
Total Absorbed Ionizing Radiation	1 mil	337 krads	506 krads	435 krads
(trapped particles, x-rays)	5 mil	96 krads	142 krads	115 krads

2.3 Observations

2.3.1 First Servicing Mission (SM1)

The first servicing mission took place in December 1993, 3.6 years after the telescope was deployed. During the mission itself, the only damage noticed was on the -V3 (anti-sun) side. Some cracks were apparent near the NASA logo, and they were attributed to the mismatch in the coefficient of thermal expansion of the materials in the MLI and the logo (Figure 5). However, close examination of the retrieved magnetometer covers revealed some localized (less than 4 cm), through-thickness cracks in areas that experienced the highest solar exposure and stress concentration [2].

The exterior of the telescope was photographed extensively during the mission, although not all surfaces were documented. At that time, it appeared that most of the MLI was intact, however, a review of those images following the second servicing mission showed more damage. A significant fraction of the largest cracks at SM2 were visible as lines or wrinkles in the older images. Following SM1 it was impossible to tell that these were crack initiation sites, however, knowing that a crack had propagated through a region at SM2, the evidence of damage could be seen in the SM1 images.

2.3.2 Second Servicing Mission (SM2)

During SM2, the first damage was noticed on the +V3 side (sun side) with several large cracks in the light shield MLI outer layer. The largest crack, more than one meter long, is shown in Figure 6. Upon further visual inspection of the vehicle, additional cracks were apparent on all MLI surfaces, on both solar and

anti-solar facing surfaces. Although the most striking damage occurred on the +V3 side, significant damage was observed all around the telescope. A program decision was made to reconfigure contingency MLI patches and use them to patch the worst of the damaged areas.

Prior to patching the corners of the Bay 8 MLI, the astronauts performed two tests: a Velcro® cycling test and a Teflon® FEP bend test. The Velcro® attaching the blanket to the spacecraft was cycled to determine its integrity. The astronauts reported that the Velcro® appeared to be securely fastened to the vehicle substrate and the hook seemed to hold the pile securely. The astronauts also bent a piece of the Teflon® FEP over on itself (VDA surface to VDA surface) to determine if manipulating it during the patching process would cause significant damage. The astronauts reported that the Teflon® FEP did not crack.

Images of the radiator surfaces revealed a mottled appearance. Figure 7 shows the aft bulkhead of the telescope during SM2. Significant increases in the solar absorptance of the silver Teflon® tape were obvious as dark patches distributed across the aft region of the telescope. Some tape strips were significantly worse than others, and the dark patches occasionally occurred in broad streaks along a section of tape.

The degradation of these thermal control materials was barely measurable as increased temperatures inside the equipment bays of the telescope. However, the telescope was designed with a large thermal margin, so at SM2 this small increase had no effect on telescope performance.

3. ANALYSIS OF RETRIEVED MATERIALS

The SM2 flight specimens were fully documented using macro photography, optical microscopy, and scanning electron microscopy (SEM). Then the MLI specimens from SM1 and SM2 were characterized through exhaustive mechanical, optical, and chemical testing.

3.1 Scanning Electron Microscopy (SEM) and Optical Microscopy

The first task was to document the SM2 LS specimen and assemble the four pieces received into the single specimen that was cut in orbit. Both SEM and optical microscopy were used in this effort. Once the original configuration had been determined, the edges were identified as either a deliberate cut, a handling artifact, or an on-orbit fracture (Figure 4). From this information, the fracture initiation site became apparent.

The fractures that resulted in the SM2 LS specimen initiated at an edge of the MLI that had been cut to fit around a handrail (Figure 3). From small defects in this cut edge, two fractures developed and propagated in orbit almost normal to one another, resulting in a roughly triangular specimen. The VDA was completely missing from the SM2 LS specimen in regions where the Teflon® FEP was bonded to the rest of the blanket, which included the region where the cracks initiated.

Although the blankets were relatively flat when deployed, photos of the SM2 LS specimen in orbit showed that it was tightly curled, with the space-exposed Teflon® FEP surface as the inner surface and the VDA exposed. This curling indicated a volume shrinkage gradient in the specimen. Based on the diameter of

the curl (1.5 cm) the estimated strain difference between the outer and inner surface of the Teflon® FEP was ~1.5% [3].

SEM images of the initiation region showed clear differences between the scissors cuts that occurred prior to launch and on orbit, the cracks that propagated while in orbit, and the cracks from subsequent handling. The fracture surface of the scissors cut surfaces showed shear and tear features (Figure 8). The orbital fracture surfaces were extremely smooth (Figure 9). Attempts to duplicate this smooth fracture with the SM2 specimen under bending or tensile stress resulted in fractures with more fibrous features (Figure 10). These fibrous cracks were found on the specimen as well, and were identified as handling cracks.

The inability to duplicate the featureless fracture indicated that the orbit fractures propagated in orbit very slowly, in the presence of relatively low stress and under the influence of radiation and other environmental factors. This type of "slow crack growth" is rather unique in polymers, and has not been studied with methods proven in studies of similar phenomenon in metals and ceramics [3].

Homogeneous mud-like cracking (mud-tiling) and buckling of the VDA were also apparent in the SEM and optical images (Figure 11). A mismatch between the coefficient of thermal expansion (CTE) of the Teflon® FEP and the VDA was most likely the cause. Tensile cracks developed in the aluminum from low cycle fatigue as the material cycled above room temperature, and buckling occurred when the material cycled below room temperature [3].

The mud-tiling of the metal backing was apparent in all of the specimens. In the SM2 CVC specimen, handling and processing procedures while adhesive bonding it to the spacecraft surface most likely created the cracks.

SEM images of the surface showed recession and texturing common in polymers exposed to a sweeping ram fluence of atomic oxygen.

3.2 Mechanical Analyses

The most obvious indication of degradation in the retrieved specimens was found in the tensile test results. Table 3 is a summary of the strength test results. In terms of strength, the SM2 LS specimen was obviously most degraded. The CVC SM2 specimen was less degraded, and the strength of the SM1 MSS specimen degraded the least. This ranking was most apparent in the elongation data. Figure 10 shows the SM2 LS tensile specimens after testing.

TABLE 3: SUMMARY OF STRENGTH TEST RESULTS (3)

Material	Yield Strength (MPa)	Ultimate Strength (MPa)	Elongation (%)
pristine	13.8	24.8	340
	14.3	26.5	360
	14.3	28.1	390
SM1 MSS	14.3	15.4	196
	14.3	16.6	116
SM2 CVC	11.0	12.1	25
	15.4	16.0	25
	N/A	11.0	15
SM2 LS	N/A	13.2	0
	N/A	2.2	0

Bend testing was performed on the retrieved specimens from SM1 and SM2. Each small specimen was bent manually to 180 degrees around successively smaller mandrels (diameters from 9.19 to 3.56 mm). Following each bend, the

specimen was examined with an optical microscope to detect crack length and features. As expected, the pristine material showed no cracking when bent around the smallest mandrel, a strain of 15 percent [4].

Each of the two SM2 LS samples formed a full-width crack when bent around the first or second large mandrel with the space-exposed surface in tension. Examination showed that this single, full-width crack went most of the way through the thickness of the sample, although the strain from the mandrel diameter was only 2 to 2.5 percent. SEM analysis of the fractures showed the fibrous features of a handling crack. Bending two other SM2 LS samples around the smallest mandrel with the space-exposed surface in compression did not produce cracks, even at the resulting 15 percent strain. This implied that the space-exposed surface was more brittle than the back surface [4].

The SM1 MSS specimens and the SM2 CVC specimens cracked quite differently from the SM2 LS specimens. Instead of a single, catastrophic crack, the specimens developed several very short, shallow cracks that eventually joined to form a long, jagged crack across the surface at much smaller mandrels (higher strain). Existing flaws from vent cuts or handling reduced the strain at which cracks first appeared. Unlike the SM2 LS samples, these samples appeared to retain considerable ductility [4].

The surface micro-hardness of the retrieved specimens were measured by Nano Instruments using their patented Continuous Stiffness Measurement technique. All of the space-exposed specimens showed an increased hardness at the surface that decreased with depth. By 500 nm, the hardness of all the exposed

specimens was indistinguishable from that of pristine at 500 nm. Although the SM1 materials seemed to show a trend of increasing hardness with increasing solar exposure, the SM2 materials, which had the highest solar exposure, did not follow this trend [4].

3.3 Optical Analyses

Significant effort was spent in determining the appropriate method for measuring the solar absorptance (α_s) of the flight materials. Because of the mud tiling and delamination of the metal coatings, traditional methods gave results that either over- or under-estimated the changes to the solar absorptance [5]. The reflectance of the specimens was measured using a Cary 5E UV-Vis-NIR Spectrophotometer with an integrating sphere (ASTM E490, E903). A 99.9 percent diffuse reflective standard was placed behind the specimens while the measurements were made to minimize light transmitted through metal delamination sites and the cracks in the specimens. The solar absorptance was then calculated by subtracting the solar reflectance from one. The details of the measurements can be found in [5].

Table 4 contains a summary of the solar absorptance data of the retrieved specimens. Since there were no control specimens from the HST lot, increases were reported with respect to pristine for the FEP/VDA specimens (SM1 MSS and SM2 LS). For the SM2 CVC specimen the post-flight increases were reported with respect to data found in literature for the solar absorptance of FEP/VDS ($\alpha_s < 0.09$).

TABLE 4: SOLAR ABSORPTANCE (α_s) OF RETRIEVED SPECIMENS (5)

Sample	# of Samples	Metallized FEP α_s	Metallized FEP Increase	FEP Alone (metal removed) α_s	FEP Alone (metal removed) Increase
Pristine	6	0.12 ± 0.002	-	0.01 ± 0.001	-
Post Flight:					
SM1 MSS	2	0.22	0.10	0.03	0.02
SM2 LS	2	0.20	0.08	0.07	0.06
SM2 CVC	2	0.125	~0.04	-	-

The majority of the absorptance increase of SM1 MSS samples are due to the crazing of the VDA [5]. For the SM2 LS specimen, most of the 0.08 solar absorptance increase of the material was attributed to increases in the solar absorptance of the Teflon® FEP, rather than to cracking in the VDA. With the VDA removed by dilute sodium hydroxide, the solar absorptance of the SM2 LS specimen was still 0.06 higher than pristine. Solar absorptance was also measured on SM1 MSS specimens that experienced varied amounts of solar exposure, and no clear correlation was found between the solar absorptance increase and equivalent solar hours (ESH) [5].

Literature values for solar absorptance of pristine FEP/VDS were found between 0.06 to less than 0.09 [10]. The increase in the solar absorptance of the SM2 CVC specimen was attributed to darkening of the acrylic adhesive that was used to bond the material to the spacecraft. During the bonding process, the material was repeatedly bent with a high angle of attack, which created the mud tiling cracks in the silver deposit. The adhesive bled through these cracks in the silver and was exposed to sunlight. Acrylic adhesives are known to darken when exposed to UV [2, 6, 10].

In these measurements, the amount of darkening varied widely as a function of the crack size and density. In localized regions of the SM2 CVC, the solar absorptance was as high as 0.14 and as low as 0.115. The average value is reported in Table 4. The average solar absorptance of the FEP/VDS on the aft region of the telescope was estimated at 0.14 based on the current on-orbit temperature data.

3.4 Chemical Analyses

The chemical composition was studied using Time-of-Flight Secondary Ion Mass Spectrometry (TOF-SIMS), Fourier Transform infrared microscopy (μ-FTIR), Attenuated Total Reflectance infrared microscopy (ATR/FTIR), and X-ray Photoelectron Spectroscopy (XPS).

Time-of-Flight Secondary Ion Mass Spectrometry (TOF-SIMS) was used to determine the ion composition of the first mono-layer (0.3 nm) of the specimens and to image ion intensities on the cross sections [6]. For pristine Teflon® FEP, the most common fragmentation point was at the bond between CF_2 molecules, and some minor contamination of the surface was found.

The SM2 LS specimen had the most evidence of chemical changes. The surface was highly oxidized, and there was weak evidence of surface de-fluorination. The cross-section analysis showed that this damage only penetrated to a depth of 5-10 μm; from 10-110 μm deep the material appeared similar to the pristine Teflon® FEP. Some silicon-containing surface contamination was also found [6].

The TOF-SIMS analysis of the SM2 CVC specimen revealed strong evidence of de-fluorination on the surface. Although oxygen was detected in a few of the

low-mass fragments, unlike the SM2 LS specimen, most ions did not contain oxygen. Analysis of the cross section showed a spectrum very similar to pristine Teflon® FEP, indicating that the de-fluorinated region was on the very surface of the specimen. Very few silicon-containing contaminants were found on this surface.

The SM1 MSS specimen most closely resembled the pristine. There was some evidence of oxidation and de-fluorination, but not to the extent present in either of the other two flight specimens. Silicon-containing contaminants were detected on the surface [6].

Fourier Transform infrared microscopy (μ-FTIR) analysis was performed as described in reference 7, to detect crystallinity changes and oxidation. The testing conducted for this effort did not confirm that this μ-FTIR method can detect crystallinity changes. So, although this method showed no significant differences in the crystallinity of the of the pristine, SM1 MSS, SM2 LS or SM2 CVC specimens, the test was inconclusive. Also, only SM1 MSS showed significant oxidation in the first 3 to 5 μm of the material [6].

X-ray Photoelectron Spectroscopy (XPS) was performed on the SM2 LS2 and CVC SM2 specimens and a pristine specimen. The analysis depth of the XPS is roughly 10 nm; a change in the ratio of carbon to fluorine (C/F) was defined as damage. The C/F ratio of pristine Teflon® FEP was 8.05 with an oxygen concentration of 0.2 atom percent. The SM2 CVC specimen appeared to be the most damaged with a measured C/F ratio of 6.3, and an oxygen concentration of 1.9 atom percent. A typical region of the SM2 LS specimen had a C/F ratio of 6.8

with an oxygen concentration of 0.8 atom percent. A region of the SM2 LS specimen that appeared contaminated was the least damaged with a measured C/F ratio of 7.9, an oxygen concentration of 1.5 atom percent, and a trace contaminant of either silicone or hydrocarbon [6].

3.5 Molecular Structure Analyses

X-ray Diffraction (XRD) was used to detect changes in the crystallinity of the returned MLI specimens from SM1 and SM2, and the results are summarized in Table 5. The pristine specimen had a crystallinity of 28-29 percent. Specimens with various ESH returned during SM1 showed a crystallinity of 28-32 percent. These measurements were within the uncertainty of the instrument, so SM1 MSS samples had a crystallinity that was indistinguishable from pristine. The SM2 LS samples showed a significant increase, with a crystallinity of 46-47 percent [6].

The density of the specimens was found using a density gradient column. This data was then converted to crystallinity values using a table provided by DuPont. These results are also summarized in Table 5. The calculated crystallinity of the SM1 specimens were indistinguishable from pristine material at 50 percent. The crystallinity of the SM2 LS2 specimen was higher, at 65 percent [6].

TABLE 5: SUMMARY OF CRYSTALLINITY AND DENSITY RESULTS

Specimen	Solar Fluence (ESH)	XRD		Density Gradient Column		
		# Tested	Crystallinity (%)	As Received Crystallinity (%)	Density (g/cm³)	Post Heating Density Change (g/cm³)
Pristine FEP	0	-	-	50	2.140	-
Pristine FEP/VDA	0	6	28-29	50	2.139	0.020
SM1 MSS	4,477	1	30	49	2.138	0.022
	6,324 or 9,193	1	29	50	2.138	0.027
	9,193 or 6,324	1	32	50	2.138	0.025
	11,339	2	29, 30	50	2.138	0.032
	16,670	1	32	50	2.141	0.031
SM2 LS	33,638	2	46, 47	65	2.184	0.001

Although there were differences between the absolute value of the crystallinity determined using XRD and the density method, the change in crystallinity is identical. Both methods show an increase in crystallinity of 15 percent. The different absolute values of the two methods was not surprising because the principles involved were so different. Based on literature data comparing XRD to various methods, a difference in absolute crystallinity of up to 14 percent is not uncommon [6].

Solid-State Nuclear Magnetic Resonance (NMR) was performed at the University of Akron on pristine Teflon® FEP and MLI specimens from SM1 and SM2 to detect changes in chemical species and morphology. NMR performed on the pristine material showed a CF_3 abundance of 7.5 percent, which remained consistent in all three specimens. Analysis of the SM1 MSS specimen detected no significant changes in chemistry or morphology. However, the morphology of the SM2 LS specimen was changed. Strong evidence was found of decreased mobility of the bonds in the specimen. Such changes are consistent with

increases in crystallinity or crystalline-like regions and with crosslinking. NMR cannot distinguish between these morphological changes.

Because the high temperature limits of the SM1 MSS and SM2 LS specimens were different once the SM2 LS specimen had curled, a few specimens of the SM1 MSS material and pristine were heated to 200 °C for several days and analyzed using NMR and density gradient column. The heated pristine material increased in density, and NMR revealed slightly decreased mobility. The heated SM1 MSS materials changed more than the heated pristine in terms of density increases and decreased mobility in NMR. This was the same type of morphological change found in the SM2 LS specimen, although the degree of change was less than was found in the SM2 LS specimen.

4. DISCUSSION

The mechanical properties of specimens that were returned from the second servicing mission were significantly degraded. Curling in the SM2 LS specimen indicated a volume shrinkage gradient through the thickness, and bend test results confirmed that the space-exposed surface was more embrittled than the inside surface. Fractographic examination of the cracks that occurred in orbit indicated that they propagated very slowly under relatively low stress in the presence of radiation or other environmental effects. Similar featureless fracture surfaces were found in the few localized cracks in the SM1 MSS specimens as well. Although it was observed on specimens retrieved during SM1, this "slow crack growth" in Teflon® has not been studied using methods proven for metals or ceramics.

Crack patterns in the vapor deposited metal coatings on the back of the thermal control materials resembled homogeneous mud cracks. This "mud tiling" can be caused by thermal cycling or handling. When the material was bonded, as with the radiator surfaces on HST, the adhesive bled through these cracks in the metal and darkened in the presence of ultraviolet radiation, increasing the solar absorptance.

The chemical analysis techniques used did not yield consistent results. TOF-SIMS data (analysis depth of 0.3 nm) indicated that the SM2 LS specimen was the most damaged, with oxygen-containing ions dominating the mass spectra. The XPS data (analysis depth of 10 nm) indicated that the SM2 CVC specimen was most changed, with the lowest C/F ratio. Infrared microscopy (analysis depth of 3 μm) was inconclusive with respect to crystallinity, although some contamination was found on the SM1 MSS specimen. The differences may have been simply a function of the analysis depths and sensitivities of the different techniques. Limited attempts to determine the chemical composition deeper into the bulk of the material with these techniques found no changes below 10 μm. Therefore, it is unlikely that composition changes (e.g. de-fluorination, oxidation) can explain the changes to the bulk properties observed in the retrieved specimens.

The decreased elongation in the retrieved specimens, as evidenced by the tensile and bend test results, demonstrated the material's loss of plastic deformation capability. This, coupled with the decreased ultimate tensile strength indicated a reduced molecular weight in the returned Teflon® FEP. This implied that chain scission, rather than crosslinking, was the dominant damage

mechanism in the retrieved materials. The density measurements and XRD analysis of the SM2 LS specimen revealed a 15 percent increase in crystallinity. The NMR analysis found no change in the bulk molecular structure of the SM1 MSS specimen and confirmed that increased crystallinity occurred in the SM2 LS specimen.

There are two possible explanations for the differences in the bulk property measurements of the SM1 and SM2 retrieved materials. The first, and simplest, is different degrees of damage. NMR and XRD both measure the bulk of a material. It is possible that, although some damage had obviously occurred, at SM1 the damage was not sufficient to be detected by these two techniques. The strength testing did reveal that the SM1 MSS specimen had decreased elongation and ultimate tensile strength, indicating chain scission. However, the damage was not as severe as at SM2.

The second explanation comes from the curling of the SM2 LS specimen. Based on the solar absorptance and emittance of the FEP/VDA, when the top layer was flat it cycled between -100 and +50 °C. Once the specimen curled such that the aluminum was exposed, the thermal properties changed significantly. With the aluminum exposed the specimen cycled between -100 and +200 °C. This higher temperature limit was only experienced by the SM2 LS specimen, not by the SM1 MSS specimen. High temperature thermal cycling can affect the crystallinity, and if the temperature is severe enough it can induce chain scission [8]. SM1 MSS materials that were heated to +200 °C in ground-based experiments increased in both density and crystallinity (NMR), although not to the degree that

the SM2 LS specimen had increased. Pristine specimens heated to +200 °C increased in density and crystallinity (NMR), but not to the same degree.

Additionally, the astronaut observation following the "bend test" in orbit revealed that a damaged region that did not curl maintained more ductility in orbit than the curled SM2 LS specimen exhibited in the ground testing. That qualitative difference could be from either the different temperatures experienced by the Bay 8 specimen and the SM2 LS specimen or from changes that occurred after the SM2 specimen was exposed to atmosphere. Further testing is required to understand the effects of atmosphere on vacuum irradiated Teflon® FEP.

Based on these results, it was apparent that exposure to some element of the space environment induced chain scission in the bulk of the material. This initial change was detected in the tensile tests, but it was masked in most other analytical techniques. When the damaged material was subjected to a high temperature extreme (+200 °C), the increased mobility of the shortened chains allowed the molecules to re-align into a more dense, crystalline structure. This change occurred in orbit when the SM2 LS specimen curled and on the ground when the SM1 MSS specimens were heated in an oven. The fact that the ground-heated SM1 MSS specimens did not become as dense or crystalline as the SM2 LS specimen indicated that the chain scission progressed over time, allowing greater mobility in the molecules of the SM2 LS specimen. With these analyses complete, the changes to the material were relatively well understood, however, what had caused these changes was not apparent.

The documentation of the condition of the blankets in various locations around HST during the two servicing missions was revealing. At the first servicing mission, there were very few macroscopic cracks. A few were discovered near the NASA logo on the anti-solar-facing side of the spacecraft, and a few were found on close examination of the returned materials from the solar-facing side. However, in general, the outer layer of the MLI blankets appeared to be intact [1,2]. During SM2, cracks all around HST were visible to astronauts and in photographs. The damage appeared to be worse on the solar-facing side of HST, but the MLI on the anti-solar side was also significantly damaged.

Note that the anti-solar-facing side of HST only received Earth albedo sunlight, equivalent to roughly 10 percent of the solar-facing equivalent solar hours (ESH) [1]. This meant that at SM1 the solar-facing surfaces of HST had received five times more ESH than the anti-solar facing surfaces had received at SM2. If any component of the ESH was the dominant damaging environmental factor, the damage to the solar-facing side should have been far worse at SM1 than the anti-solar facing surfaces. The photographic evidence of HST clearly contradicts this supposition.

Several different simulations were employed individually and in combination to determine which elements of the space environment were most likely to cause the damage observed in the returned specimens. Based on the results from synchrotron radiation exposures, it was clear that neither VUV nor soft X-ray radiation alone could cause the observed bulk damage to the HST thermal control materials [6]. Continuum soft x-ray exposures conducted in an

electron beam facility with higher energy x-rays provided consistent results. These wavelengths did reduce elongation at extremely high fluences, however, even at doses several orders of magnitude higher than experienced by HST at SM2 there were no comparable bulk property changes. These results, coupled with the damage map of HST, cast strong doubt on the idea that any component of the solar spectrum could be solely responsible for the damage observed on HST.

Because the damage to HST did not appear to coincide with ESH, components of the space environment that are more closely homogeneous were suspect. The likely candidates were electron and proton fluences and thermal cycling. Experiments showed that electron and proton radiation alone affected the tensile properties of the Teflon® FEP. The reduced ultimate strength and elongation was apparent at fluences comparable to the HST end-of-life (20 years). Subsequent thermal cycling between -100 and +60 °C reduced these properties further. These particle radiation exposures coupled with thermal cycling produced damage that most closely resembled the HST specimens. However, the study did not duplicate the degree of damage observed on the returned SM2 specimen with SM2 doses of radiation and thermal cycling at nominal limits (-100 to +50 °C) [9].

Since the thermal cycling following irradiation did affect the tensile properties of the materials and the crystallinity was strongly affected by temperature, it is likely that the more extreme thermal cycling the SM2 LS specimen experienced produced more damage. Further testing is needed to determine what effect the high temperature cycling has on irradiated Teflon® FEP.

5. CONCLUSIONS

Analysis showed that all of the retrieved specimens, SM1 MSS, SM2 LS and SM2 CVC, underwent chain scission. Evidence of increased crystallinity was found only in the SM2 LS specimen, and was generated by heating SM1 MSS specimens. Solar absorptance increases in the SM2 LS specimen were attributed to these changes in the Teflon® FEP and mud tiling in the VDA. Solar absorptance increases in the SM2 CVC specimen were attributed to mud tiling from handling and subsequent darkening of the acrylic adhesive.

The conclusions of the HST MLI Failure Review Board were based on the combined evidence of HST damage and data uncovered in ground-based experiments. The Failure Review Board concluded the following:

> *The observations of HST MLI and ground testing of pristine samples indicate that thermal cycling with deep-layer damage from electron and proton radiation are necessary to cause the observed Teflon® FEP embrittlement and the propagation of cracks along stress concentrations. Ground testing and analysis of retrieved MLI indicate that damage increases with the combined total dose of electrons, protons, UV and x-rays along with thermal cycling.*

Tests continue in order to determine the effects of the higher temperature limit that the SM2 LS2 specimen experienced.

ACKNOWLEDGMENTS

The analysts in the Materials Engineering Branch of NASA, Goddard Space Flight Center who performed tests are Diane Kolos, Charles Powers, Bruno Munoz (Unisys), Alex Montoya, Mary Ayres-Treusdell, Tom Zuby (Unisys), and Mike Viens. Other GSFC contributors include Steve Brown, Claude Smith, Bob Gorman, Wanda Peters (Swales), Dave Hughes (Swales), and Jack Triolo (Swales). The fluence and dose calculations were performed by Janet Barth (GSFC), Teri Gregory (Lockheed), and Shaun Thomson (GSFC). Analysts at NASA, Lewis Research Center who performed tests are Don Wheeler, and Jim Gaier. The TOF-SIMS analysis was performed under contract by Mark Nicholas of Evans East. The Nano Indenter analysis was performed by Barry Lucas and Angela Gizelar of Nano Instruments, Inc. NMR analysis was performed by Matthew Espe and Daveen England of the University of Akron. The work of all these analysts and the contributions of the entire HST MLI Failure Review Board are gratefully acknowledged by the authors.

REFERENCES

1. Zuby T, de Groh K, and Smith D 1995 "Degradation of FEP Thermal Control Materials Returned from the Hubble Space Telescope", NASA Technical Memorandum 104627
2. Hansen PA, Townsend JA, Yoshikawa Y, Castro JD, Triolo JJ, and Peters WC 1998 "Degradation of Hubble Space Telescope Metallized Teflon® FEP Thermal Control Materials", Science of Advanced Materials and Process Engineering Series, 43, 570-81
3. Wang L, Viens M, and Townsend J 1998 "Mechanical Properties and Fractography of MLI FEP from the HST Second Service Mission", Science of Advanced Materials and Process Engineering Series, 43, 594-606
4. Dever JA, de Groh KK, Townsend JA, and Wang LL 1998 "Mechanical Properties Degradation of Teflon® FEP Returned from the Hubble Space Telescope", NASA/TM-1998-206618
5. He C and Townsend JA 1998 "Solar Absorptance of the Teflon® FEP Samples Returned from the HST Servicing Missions", Science of Advanced Materials and Process Engineering Series, 43, 607-15
6. Townsend JA, Hansen PA, Dever JA, and Triolo JJ 1998, "Analysis of Retrieved Hubble Space Telescope Thermal Control Materials", Science of Advanced Materials and Process Engineering Series, 43, 582-93
7. Milintchouk A, Van Eesbeek M, Levadou F, and Harper T 1997 *J. Spacecraft and Rockets,* **34:4** , 542-548

8. Mark, HF (1983) "Degradation of Polymers in Hostile Environments", The Effects of Hostile Environments on Coatings and Plastics, American Chemical Society Symposium Series 229, 11-5

9. Townsend JA, Powers CE, Viens MJ, Ayers-Treusdell MT, and Munoz BF 1998 "Degradation of Teflon® FEP Following Charged Particle Radiation and Rapid Thermal Cycling", To be published in 20th Space Simulations Conference Proceedings

10. Hermans PH and Weidinger A 1948 *J. Appl. Phy.*, **19,** 491

ILLUSTRATIONS

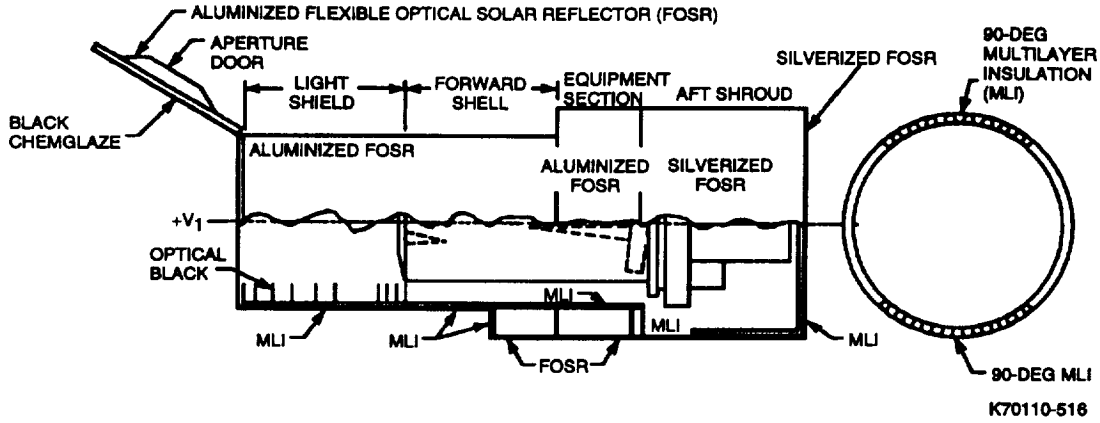

FIGURE 1: LOCATION OF HUBBLE SPACE TELESCOPE THERMAL CONTROL MATERIALS
In this image, Flexible Optical Solar Reflector (FOSR) is defined as metallized Teflon films used either as the top layer of MLI blankets or as tapes on radiator surfaces. MLI blankets were used on the entire Light Shield and most of the Forward Shell and Equipment Bays (Equipment Section). Tapes were used on the Aperture Door, a few locations on Equipment Bays, the entire Aft Shroud, and Aft Bulkhead (bottom of the telescope).

FIGURE 2: SM1 MAGNETIC SENSING SYSTEM (MSS) SPECIMEN ON-ORBIT

The top-right of this image shows one of the two magnetic sensing system (MSS) covers while still in place on the light shield region of HST. This is an image from SM1 of the region that had the worst damage at SM2 (see Figure 3).

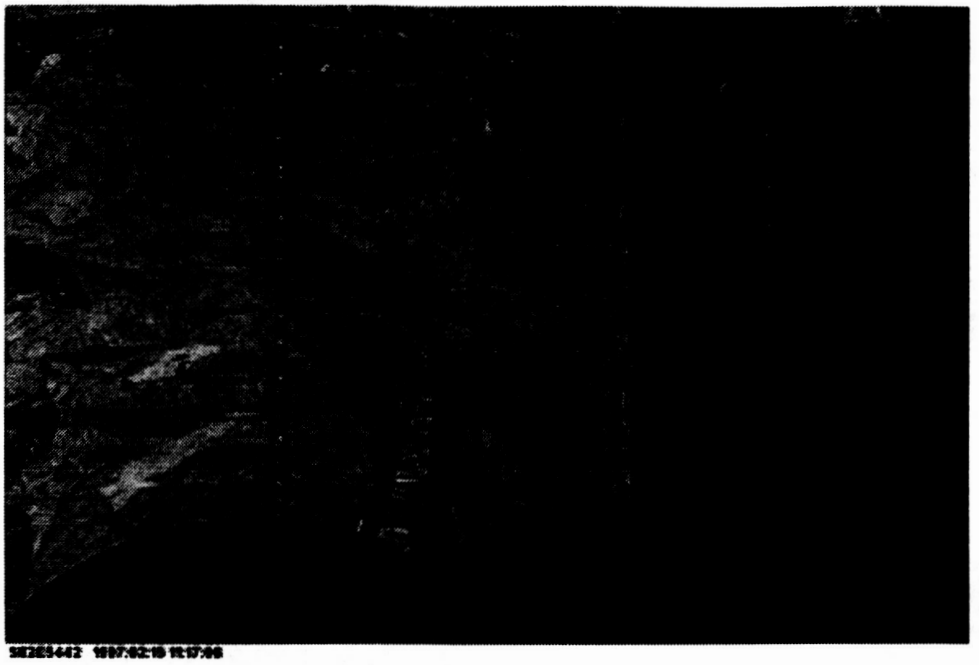

FIGURE 3: SM2 LS SPECIMEN ON-ORBIT

The top-center of this image shows the roughly triangular SM2 LS specimen on the Light Shield at SM2 prior to retrieval. A handrail and standoffs are apparent across the top of the image. The specimen is curled very tightly, so that it is detectable here as a triangular region where the next layer of the MLI is visible. The raised feature at the bottom edge of the triangular opening contains the entire specimen that covered this triangle prior to the damage. At the bottom of the image, the tip of the largest crack on HST is seen propagating vertically towards the top of the telescope. This large crack also opened to reveal the next MLI layer.

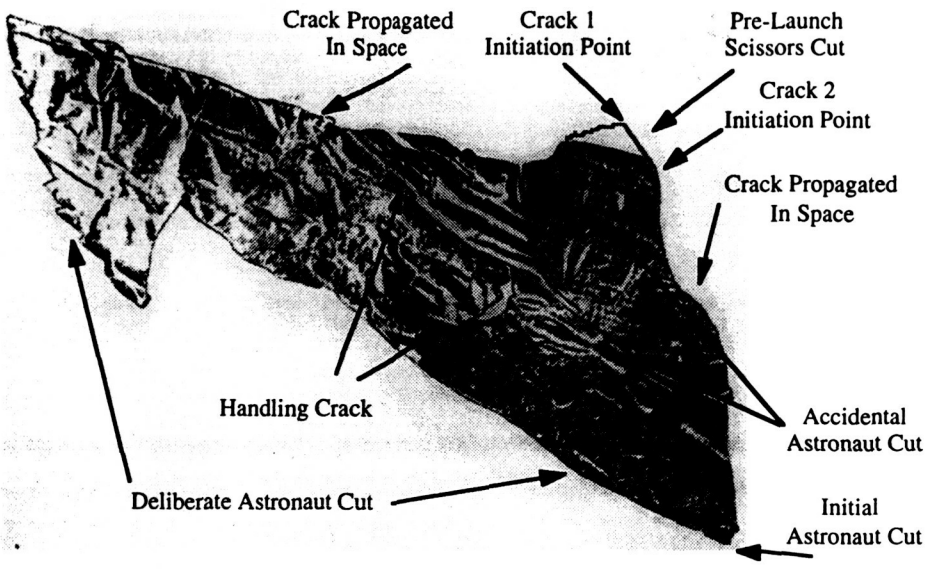

FIGURE 4: SM2 LS SPECIMEN POST-RETRIEVAL

The image above was taken during post-retrieval analysis, when the SM2 LS specimen was uncurled and placed between glass plates. The edges of the specimen are identified as scissors cut, handling crack, or orbit crack. The top-right corner of the specimen contains the crack initiation sites.

FIGURE 5: SM1 ANTI-SOLAR FACING SIDE WITH NASA LOGO

This image shows the only noticeable damage to the MLI during SM1. Note the peeling in the NASA logo and cracks radiating away from the logo. Much more damage had occurred on this side of the telescope by SM2.

FIGURE 6. ASTRONAUTS PATCH THE HST LIGHT SHIELD DURING SM2

This image shows two astronauts in the process of patching the Light Shield MLI during SM2. The astronauts give scale to the largest crack (more than one meter long) in the MLI at SM2. At this point the SM2 LS specimen had already been removed (left of top left black corner).

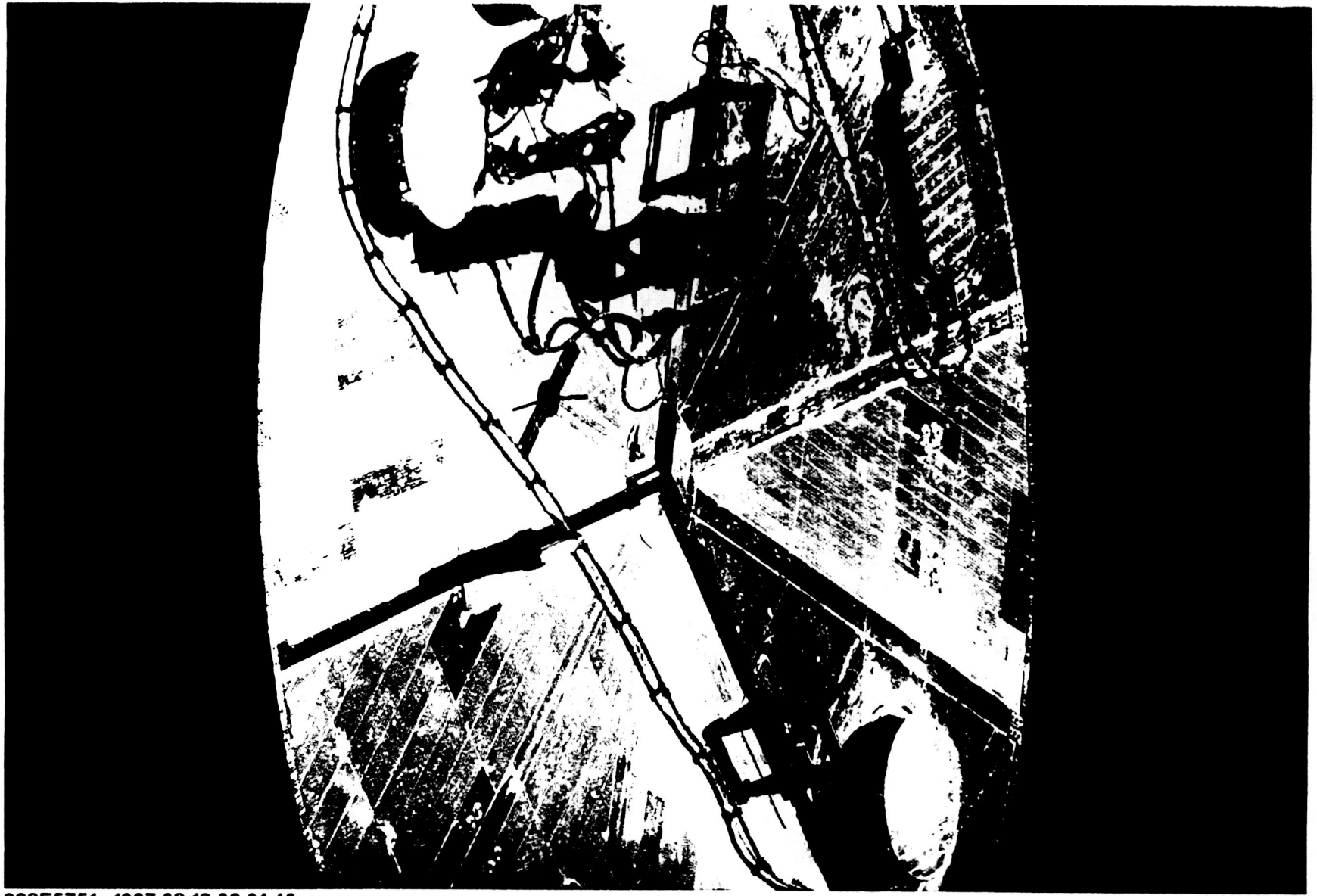

S82E5751 1997:02:13 08:01:40

FIGURE 7: SM2 AFT BULKHEAD

The radiator surfaces of the telescope had this mottled appearance showing localized increases in solar absorptance from UV darkening of the acrylic adhesives.

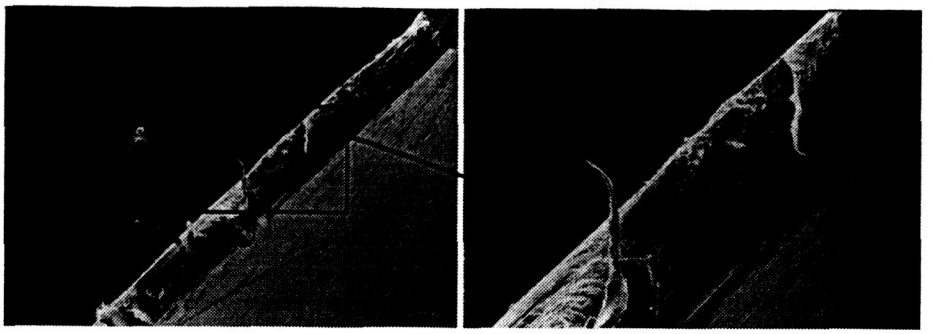

300X

Figure 8: SM2 LS Specimen Scissors Cut Features

Edge-on view of shear fracture near the crack initiation point. This region of the blanket was cut during installation in order to fit around a handrail. This fracture surface has common shear and tear features, indicating the material was cut. Astronaut cuts that occurred on-orbit during specimen retrieval had a similar appearance.

5000X

Figure 9: SM2 LS Specimen On-Orbit Crack Propagation Features

Edge-on view of the crack that occurred in space near the crack initiation point. The unique, extremely smooth features indicated the crack was a form of environmentally assisted slow crack growth. These smooth features could not be duplicated by handling the specimen. This allowed for easy identification of fractures that occurred on-orbit.

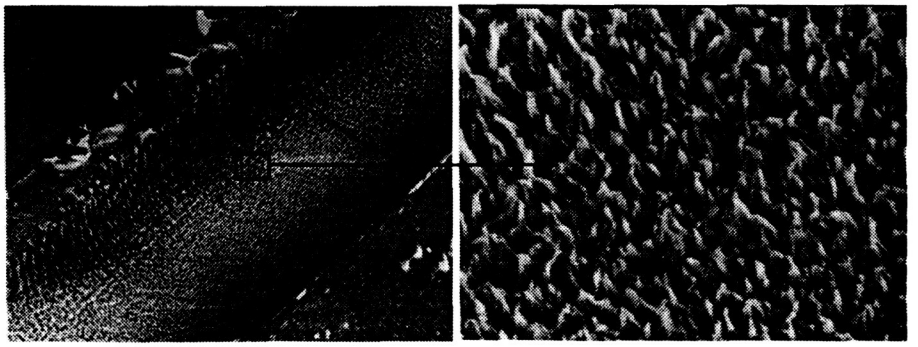

5000X

Figure 10: SM2 LS Specimen Handling Features

Edge-on view of a crack that occurred due to specimen handling. The fibrous features of this crack surface showed ductile peaks that formed as the two surfaces of the crack pulled away from one another. Cracks that occurred from tensile and bend testing had a similar appearance.

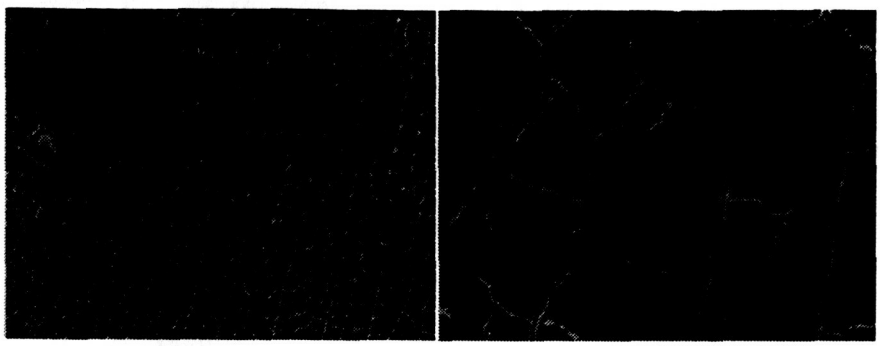

100X 800X

Figure 11: SM2 LS Specimen Mud-Tiling Features

SEM image of the VDA surface of the retrieved specimen. These cracks in the aluminum occurred due to the mismatch in the coefficient of thermal expansion (CTE) of aluminum and Teflon FEP.